Fourier-Ray Modeling of Transient Trapped Lee Waves

Dave Broutman and Jun Ma

Computational Physics, Inc., Springfield, Virginia

Stephen D. Eckermann

E. O. Hulburt Center for Space Research, Naval Research Laboratory, Washington, D.C.

John Lindeman

School of Computational Sciences, George Mason University, Fairfax, Virginia

ABSTRACT

The Fourier-ray method involves ray tracing in a Fourier-transform domain. The ray solutions are then Fourier synthesized to produce a spatial solution. Here previous steady-state developments of the Fourier-ray method are extended to include a transient source of mountain waves. The method is illustrated with an initial value problem in which the background flow is started abruptly from rest and then maintained at steady velocity. The resulting wave transience is modeled in a simple way. All rays that radiate from the mountain, including the initial rays, are assigned the full amplitude of the longtime steady-state solution. Time dependence comes in through the changing position of the initial rays. This is sufficient to account for wave transience in a test case, as demonstrated by comparison with simulations from a mesoscale numerical model.

1. Introduction

Ray solutions are often expressed in spatial coordinates. Some examples for mountain waves are given in Gjevik and Marthinsen (1978), Hines (1988), Shutts (1998), and Broad (1999). Ray solutions can also be expressed in Fourier-transform coordinates and then mapped into a spatial solution by inverse Fourier transform. For waves in a height-dependent background, the use of Fourier transform coordinates simplifies important parts of the ray calculation, including the ray initialization, the ray tracing itself, and the correction of caustics.

We believe this method has promise for mountain-wave forecasting. Three-dimensional solutions can be calculated in minutes on a standard (1 GHz) processor, and at much higher resolution than is practical with a mesoscale model. The method handles vertical directional wind shear in the presence of turning points (Broutman et al. 2003) and critical layers (Broutman et al. 2002). However, it does not treat finite-amplitude effects, boundary layer effects, flow blocking, or horizontally nonuniform backgrounds.

Previous applications of the method have been restricted to longtime steady-state solutions (Broutman et al. 2002, 2003). Here we develop a time-dependent formulation that follows the evolution of a transient wave field. This can lead to improved forecasts and is useful for interpreting observations and numerical models. There are computational benefits as well, since the transient solution can sometimes be represented on a smaller grid and does not have the resonant singularities associated with the trapped waves of the steady-state solution (see section 2d).

We consider an initial value problem in which the background flow is started abruptly from rest and then maintained at a steady velocity. The resulting wave transience is modeled in a simple way. All rays that emerge from the mountain, including the initial rays, are assigned the full wave amplitude of the longtime steady-state ray solution. The time dependence comes

Corresponding author address: Stephen Eckermann, E. O. Hulburt Center for Space Research, Naval Research Laboratory, Code 7646, Washington, DC 20375.
E-mail: stephen.eckermann@nrl.navy.mil

		Form Approved *OMB No. 0704-0188*
Report Documentation Page		

Public reporting burden for the collection of information is estimated to average 1 hour per response, including the time for reviewing instructions, searching existing data sources, gathering and maintaining the data needed, and completing and reviewing the collection of information. Send comments regarding this burden estimate or any other aspect of this collection of information, including suggestions for reducing this burden, to Washington Headquarters Services, Directorate for Information Operations and Reports, 1215 Jefferson Davis Highway, Suite 1204, Arlington VA 22202-4302. Respondents should be aware that notwithstanding any other provision of law, no person shall be subject to a penalty for failing to comply with a collection of information if it does not display a currently valid OMB control number.

1. REPORT DATE **FEB 2006**	2. REPORT TYPE	3. DATES COVERED **00-00-2006 to 00-00-2006**
4. TITLE AND SUBTITLE **Fourier-Ray Modeling of Transient Trapped Lee Waves**		5a. CONTRACT NUMBER
		5b. GRANT NUMBER
		5c. PROGRAM ELEMENT NUMBER
6. AUTHOR(S)		5d. PROJECT NUMBER
		5e. TASK NUMBER
		5f. WORK UNIT NUMBER
7. PERFORMING ORGANIZATION NAME(S) AND ADDRESS(ES) **Naval Research Laboratory,E. O. Hulburt Center for Space Research,Code 7646,Washington,DC,20375**		8. PERFORMING ORGANIZATION REPORT NUMBER
9. SPONSORING/MONITORING AGENCY NAME(S) AND ADDRESS(ES)		10. SPONSOR/MONITOR'S ACRONYM(S)
		11. SPONSOR/MONITOR'S REPORT NUMBER(S)
12. DISTRIBUTION/AVAILABILITY STATEMENT **Approved for public release; distribution unlimited**		
13. SUPPLEMENTARY NOTES		

14. ABSTRACT

The Fourier-ray method involves ray tracing in a Fourier-transform domain. The ray solutions are then Fourier synthesized to produce a spatial solution. Here previous steady-state developments of the Fourierray method are extended to include a transient source of mountain waves. The method is illustrated with an initial value problem in which the background flow is started abruptly from rest and then maintained at steady velocity. The resulting wave transience is modeled in a simple way. All rays that radiate from the mountain, including the initial rays, are assigned the full amplitude of the longtime steady-state solution. Time dependence comes in through the changing position of the initial rays. This is sufficient to account for wave transience in a test case, as demonstrated by comparison with simulations from a mesoscale numerical model.

15. SUBJECT TERMS					
16. SECURITY CLASSIFICATION OF:			17. LIMITATION OF ABSTRACT	18. NUMBER OF PAGES	19a. NAME OF RESPONSIBLE PERSON
a. REPORT **unclassified**	b. ABSTRACT **unclassified**	c. THIS PAGE **unclassified**	**Same as Report (SAR)**	**8**	

in through the changing position of the initial rays. This approach gives a reasonable representation of the evolving wave field, as demonstated in section 3 by comparison with a mesoscale numerical model in an idealized case. A demonstration for a more realistic case is given in Eckermann et al. (2006) for mountain waves generated by the island of Jan Mayen.

Our theory relates to a transient source of waves, not a transient background wind or stratification. We do envision an instant start-up of the wind but only as a means to generate an evolving wave field. To properly accommodate a transient background we would have to allow variations in the wave frequency along the ray (e.g., Lott and Teitelbaum 1993), and we would have to deal with a more general range of caustic conditions.

We refer to the present method as the Fourier-ray method to indicate that the spatial solution is obtained by a Fourier synthesis of ray solutions. This is the third name that has been used for the same basic approach in three papers. The reasons for the name changes are discussed at the end of section 2.

2. Theory

We modify the derivation of the Fourier-ray method in Broutman et al. (2003) to allow for wave transience. We consider an initial value problem in which the wind is imposed abruptly at time $t = 0$. All rays, including the initial rays, are treated as though their wave amplitudes instantly satisfy the steady-state solution for wave-action conservation. The theory does allow for a gradual ramping up of the wave amplitude to a steady-state value, rather than an instantaneous growth to the full steady-state value, but we have found that the latter is sufficient to obtain a good comparison with numerical simulations.

The coordinate system is $\mathbf{x} = (x, y, z)$ with z vertical. The background wind is $\mathbf{U} = [U(z), V(z), 0]$, and the buoyancy frequency is $N(z)$. For the mountain waves, $\mathbf{k} = (k, l, \pm m)$ is the wavenumber vector, and $\hat{\omega} = -kU - lV$ is the intrinsic frequency. Our notation is that $m \geq 0$, with a minus sign preceding m when it is appropriate to indicate waves with downward phase velocity and upward group velocity. The gravity wave dispersion relation is

$$m^2 = (k^2 + l^2)(N^2/\hat{\omega}^2 - 1). \quad (1)$$

We have ignored the effects of compressibility and the earth's rotation in (1). The usual density scaling of the wave amplitudes can be incorporated into the theory through (8) in order to to account for the decrease in atmospheric density with height. This is done in Eck-

ermann et al. (2006), but the results presented in section 3 below are calculated in the Boussinesq limit.

We express the ray solution in Fourier-transform coordinates, with the Fourier transform taken over the horizontal coordinates only. The ray solution is thus a function of k, l, z, and time t. Its inverse Fourier transform yields an appoximation for the spatial wave solution. An advantage of using Fourier-transform coordinates for the ray tracing instead of the more usual spatial coordinates is that k and l are constant along each ray in a horizontally uniform background, as assumed here. This reduces most of the problem to a one-dimensional calculation as a function of z. There is also time dependence, which comes into the calculation only in tracking the height of the initial rays.

We work here in terms of the vertical displacement, denoted by $\eta(x, y, z, t)$ in spatial coordinates and by $\tilde{\eta}(k, l, z, t)$ in Fourier-transform coordinates. The former is the inverse Fourier transform of the latter:

$$\eta(x, y, z, t) = \int\int_{-\infty}^{\infty} \tilde{\eta}(k, l, z, t)e^{\iota(kx+ly)}\, dk\, dl. \quad (2)$$

In the following derivation, we treat two types of waves separately: propagating waves without turning points, denoted by $\tilde{\eta}_{\mathrm{pr}}$, and (vertically) trapped waves with turning points, denoted by $\tilde{\eta}_{\mathrm{tr}}$. Thus,

$$\tilde{\eta} = \tilde{\eta}_{\mathrm{pr}} + \tilde{\eta}_{\mathrm{tr}}. \quad (3)$$

It is also convenient to divide the trapped waves into contributions from upgoing and downgoing rays:

$$\tilde{\eta}_{\mathrm{tr}} = \tilde{\eta}_{\mathrm{up}} + \tilde{\eta}_{\mathrm{dn}}. \quad (4)$$

a. Propagating waves

The solution for the vertically propagating waves has the form

$$\tilde{\eta}_{\mathrm{pr}}(k, l, z, t) = F\tilde{h}(G_0/G)^{1/2}e^{i\phi}. \quad (5)$$

Except for the factor F, which is an amplitude modulation function used to account for wave transience, this is the same form for the ray solution as the one derived for propagating waves in Broutman et al. (2003). We now define the terms in (5).

The wave phase in (5) is given by

$$\phi(k, l, z) = -\int_0^z m(k, l, z')\, dz', \quad (6)$$

and G is defined by

$$G = \rho N^2 c_{g3}/\hat{\omega}, \quad (7)$$

with $G_0 \equiv G(z = 0)$. The vertical group velocity is $c_{g3} \equiv \partial\hat{\omega}/\partial m$, and the background density is $\rho(z)$.

The term $(G_0/G)^{1/2}$ in (5) ensures that, apart from the transient effects modeled by F, the waves satisfy the constancy of the vertical flux of wave action

$$\rho c_{g3}\tilde{A} = \text{constant}, \tag{8}$$

where $\tilde{A} = |\tilde{\eta}|^2 N^2/\hat{\omega}$ is the wave-action density per unit mass. This constancy of the vertical flux of wave action is satisfied only in the Fourier transform domain. The waves in the spatial domain disperse horizontally, as well as vertically, and therefore do not preserve their vertical flux of wave action. For a form of the wave-action solution that includes the effects of horizontal and vertical dispersion (see Shutts 1998; Broad 1999).

We have assumed that the waves satisfy the linearized lower boundary condition

$$\tilde{\eta}(k, l, z = 0) = \tilde{h}(k, l), \tag{9}$$

where $\tilde{h}(k, l)$ is the Fourier transform of the topography $h(x, y)$.

We incorporate wave transience through the function $F(k, l, z, t)$ in (5). This is the only quantity on the right-hand side of (5) that depends on time. It can be used to turn the wave amplitude on or off, gradually or instantly. For the present application, we turn the wave amplitude on instantly and permanently. That is, we assume that the waves are generated from an initial state of rest at $t = 0$, and we assign the full wave amplitude of the steady-state solution to every ray. Thus, we set

$$F(k, l, z, t) = H\left[\int_0^t c_{g3}(k, l, z)\, dt' - z\right]. \tag{10}$$

The Heaviside function $H(\xi)$ is zero for $\xi < 0$ and unity for $\xi > 0$. The integral in the argument of H is the height at time t of the initial ray (for each k, l) generated at the mountain at $t = 0$.

b. Trapped waves

Trapped rays continually reflect between the ground and the turning-point height z_t, where $\hat{\omega} = N$. For each reflection, a new term must be added to the ray solution. Each new term is a copy of the previous term, but phase shifted by the amount

$$\Phi = 2\hat{\phi} - \pi/2. \tag{11}$$

Here

$$\hat{\phi} = -\int_0^{z_t} m\, dz, \tag{12}$$

is the change in phase for propagation from the ground to the turning-point height $z_t(k, l)$. The factor of $-\pi/2$ in (11) is the sum of two phase shifts: the phase shift of $+\pi/2$ due to reflection from the turning point, and the phase shift of $-\pi$ due to reflection from the ground. [The turning-point phase shift is given on p. 397 of Lighthill (1978) and in section 10.1.3 of Kravtsov and Orlov(1999).]

Thus, after the initial ray crosses z on its way up M_1 times, the ray solution for the upgoing rays is

$$\tilde{\eta}_{\text{up}} = \tilde{h}(G_0/G)^{1/2}e^{\iota\phi}S_{M_1}. \tag{13}$$

The sum $S_M(k, l, z)$ is defined by

$$S_M = \sum_{n=0}^{M-1} e^{\iota n(\Phi + \iota\alpha)}, \tag{14}$$

$$= \frac{1 - e^{\iota M(\Phi + \iota\alpha)}}{1 - e^{\iota(\Phi + \iota\alpha)}}, \tag{15}$$

with $M = M_1$ for the upgoing rays and $M = M_2$ for the downgoing rays (see below). When $M_1 = 0$, that is, before the initial ray crosses z for the first time, S_{M_1} is defined to be zero.

The positive constant α in the expression for S represents damping. The results we present in the next section are inviscid ($\alpha = 0$), but we have included this damping term to use in an intermediate step of a derivation below (section 2d), and because it might be useful in other applications. For example, Smith et al. (2002) applied the same form of damping to parameterize the partial absorption of trapped waves by a stagnant lower boundary layer. The problem was reexamined by Smith et al. (2006), who found that a better description of the process should include, in addition to damping, a phase shift different from π in the wave reflected from the boundary layer. The phase shift can be incorporated in the present model with an imaginary part for α.

After the initial ray crosses the height z on its way down M_2 times, the ray solution for the downgoing rays is

$$\tilde{\eta}_{\text{dn}} = \iota\tilde{h}(G_0/G)^{1/2}e^{\iota\phi_2}S_{M_2}. \tag{16}$$

Here ϕ_2 is the phase of the initial ray after its first reflection from the turning point but before its first reflection from the ground. We include the $\pi/2$ phase shift from the first turning-point reflection as the factor of ι at the start of the right-hand side of (16). This leaves

$$\phi_2 = \hat{\phi} - \int_z^{z_t} m(k, l, z')\, dz'. \tag{17}$$

The sum S_{M_2} in (16) is given by (14) with $M = M_2$.

Wave transience thus comes in through the crossing numbers M_1 and M_2, which are functions of k, l and which increase in a step-function manner with time. Either $M_1 = M_2 + 1$, if the initial ray has just crossed z on its way up, or $M_1 = M_2$ if the initial ray has just crossed z on its way down.

Our most general form for the ray solution for the trapped waves is then

$$\tilde{\eta}_{\text{tr}} = \tilde{h}(G_0/G)^{1/2}(e^{\iota\phi}S_{M_1} + \iota e^{\iota\phi_2}S_{M_2}). \quad (18)$$

c. Caustic correction for the trapped waves

At a turning point, the ray solution (18) diverges because c_{g3}, and hence G, vanish. This is a caustic singularity. The simplest caustics are correctable with an Airy function. One can either match the ray solution to the Airy function at a position near the caustic (e.g., section 4.11 of Lighthill 1978), or combine the ray solution and the Airy function into a uniform representation that is valid close to, and far from, the caustic (e.g., section 10.1.3 of Kravtsov and Orlov 1999). The latter method is simple to implement, so we will use it here.

We first consider one pair of rays, incident upon and reflected from the caustic, with solutions of the form $A \exp(\iota\phi_1)$ and $iA \exp(\iota\phi_2)$, respectively. The factor of ι in the reflected wave solution accounts for the phase shift of $\pi/2$ at the caustic. The uniform solution is (section 10.1.3 of Kravtsov and Orlov 1999)

$$u = 2\iota\pi^{1/2}(-r)^{1/4}A\text{Ai}(r)e^{i(\xi - \pi/4)}, \quad (19)$$

where

$$\xi = \frac{1}{2}(\phi_1 + \phi_2), \quad (20)$$

$$r = -\left[\frac{3}{4}(\phi_1 - \phi_2)\right]^{2/3}. \quad (21)$$

The Airy function argument r is zero at the caustic, negative in the propagating region below the caustic, and positive in the evanescent region above the caustic.

When there are M_2 downgoing rays, there are also M_2 pairs of incident and reflected rays. We can accommodate M_2 pairs by again introducing the sum S_{M_2}, so that the uniform solution is

$$\tilde{\eta}_u = 2\iota\pi^{1/2}(-r)^{1/4}A\text{Ai}(r)e^{\iota(\xi - \pi/4)}S_{M_2}, \quad (22)$$

with $A = \tilde{h}(G_0/G)^{1/2}$.

If $M_1 = M_2 + 1$, the initial ray is on its way up to the turning point and is not paired with a reflected ray from the turning point. It thus needs to be counted separately

from the uniform solution. The trapped wave solution can then be written as

$$\tilde{\eta}_{\text{tr}} = \tilde{\eta}_u + (M_1 - M_2)\tilde{h}(G_0/G)^{1/2}e^{\iota(\phi + M_2\Phi)}, \quad (23)$$

where $\tilde{\eta}_u$ is given by (22). When $M_1 = M_2$ each ray incident on the turning point is paired with a ray reflected from the turning point. Otherwise the second term above accounts for the initial ray.

d. Steady-state solutions

Our time-dependent solution for the trapped waves approaches the steady-state solution of Broutman et al. (2003) in the infinite-time limit. This can be shown by letting M_1 and M_2 approach infinity and introducing a small amount of damping in (15), through the positive constant α, so that the sums S_{M_1} and S_{M_2} converge. Substituting (15) into (18) and letting $\alpha \to 0$ gives, after some algebra,

$$\tilde{\eta}_{\text{tr}}(k,l,z,t \to \infty) = \tilde{h}\left(\frac{G_0}{G}\right)^{1/2}\frac{\sin(\hat{\phi} - \phi - \pi/4)}{\sin(\hat{\phi} - \pi/4)}. \quad (24)$$

This agrees with (18) of Broutman et al. (2003). For the uniform solution (22), the limit of M_1 and M_2 approaching infinity gives, after some algebra,

$$\tilde{\eta}_u(k,l,z,t \to \infty) = \tilde{h}\left(\frac{G_0}{G}\right)^{1/2}\left(\frac{r}{r_0}\right)^{1/4}\frac{\text{Ai}(r)}{\text{Ai}(r_0)}. \quad (25)$$

This agrees with (A9) of Broutman et al. (2003).

Some of our expressions for the transient solutions can be expressed in terms of a time-dependent factor times the steady-state solution. But the computational disadvantage of doing this is that the steady-state solution contains resonant singularities. These occur for those k, l values for which the reflected rays are perfectly in phase with each other. They correspond to the zeros of $\sin(\hat{\phi} - \pi/4)$ in (24) and to the zeros $Ai(r_0)$ in (25). A small imaginary component added to the wavenumber (or frequency) eliminates this singularity, as was done in Broutman et al. (2003), but this also damps the solution. No such singularities exist in the time-dependent solutions, and there is no associated damping in our solutions.

e. Terminology

As noted in the introduction, three different names have been applied to the same basic method used here of synthesizing ray solutions by inverse Fourier transform.

In Broutman et al. (2002), the method was called Maslov's method, after a Russian mathematician whose work is summarized by Maslov and Fedoriuk (1981)

and at a more understandable level by Brown (2000). The idea is that as the rays are mapped between the spatial and Fourier-transform domains, the locations of caustics change. In some cases the caustics in one domain disappear entirely in the other domain. This occurs in the hydrostatic mountain-wave model studied by Broutman et al. (2002). They derived the ray solution in the spatial domain, then mapped it into a ray solution in the Fourier transform domain using the ray relation between position and wavenumber. They then mapped back to the spatial domain by inverse Fourier transform. This sequential use of different types of mappings—first by the ray relations, then by inverse Fourier transform—is why one finishes with a different spatial solution than the original spatial ray solution.

This is the approach developed originally by Maslov. But the application of Broutman et al. (2002) was simple: there were no caustics in the Fourier-transform domain, and furthermore the problem was separable, and thereby reducible to a one-dimensional calculation in the Fourier-transform domain. Maslov is recognized for his work on the more complicated case of nonseparable problems with caustics in both the spatial and Fourier-transform domains, as in the application to surface gravity waves by Brown (2000).

So in the study of Broutman et al. (2003), the name was changed to a "simplified Fourier method" (see also Broutman and Rottman 2004). The Fourier method in this context is a Fourier synthesis of the vertical eigenfunctions, and the simplification refers to that fact that the vertical eigenfunctions were approximated by ray theory. In the present paper, we changed the name yet again to the "Fourier-ray method" in order to emphasize the involvement of ray theory and its enhanced role here in predicting the evolving positions of the leading rays for the time-dependent solutions.

3. Results

For a test case, we consider the model of Wurtele et al. (1987, hereafter WSK). The stratification is uniform, and the mountain waves are trapped by a horizontal wind that increases linearly with height. We have already used this model for a test case in the steady-state theory of Broutman et al. (2003). As in that paper, we use a nonlinear mesoscale model for verification. It has a standard second-order finite-difference discretization of the nonlinear nonhydrostatic equations of motion, in either the anelastic approximation or, as used here, the Boussinesq approximation. The model is essentially the same as that described in Lipps and Hemler (1982).

The topography is

$$h(x,y) = h_0 a^3/(x^2 + y^2 + a^2)^{3/2}, \quad (26)$$

with Fourier transform

$$\tilde{h}(k,l) = (h_0 a^2/2\pi) \exp[-a(k^2 + l^2)^{1/2}]. \quad (27)$$

The mean wind is given by

$$U(z) = U_0(1 + z/L), \quad (28)$$

where U_0 and L are constants. The y-component V of the wind is zero. We consider the tropospheric model in WSK's section 2a with the parameter values of WSK's case II. These are $N = 0.01$ s^{-1}, $a = 2.5$ km, $h_0 = 100$ m, $L = 2.5$ km, and $U_0 = 10$ m s^{-1}.

To determine M_1 and M_2, the time-dependent numbers of upgoing and downgoing rays, we have found it adequate to use the following approximation. Each time the initial ray (generated at the mountain at $t = 0$) makes one complete round trip from the ground to the turning point and back again, we increase both M_1 and M_2 by one. We use a rounded estimate given by

$$M_1 = M_2 = \text{round}(t/2T), \quad (29)$$

where T is the propagation time from the ground to the turning point, and $t/2T$ is rounded to the nearest integer.

The expression for T can be derived from the ray equation $dm/dt = -kU_z$, where d/dt is the rate of change following the ray (Lighthill 1978). Using (28), the ray equation integrates to $m = m_0 - kU_0t/L$. Letting $m_0 \equiv m(z = 0)$, and identifying $m = 0$ as the vertical wavenumber at the turning point, we have

$$T = m_0 L/kU_0 \quad (30)$$

for the propagation time from the ground to the turning point.

We show solutions for the vertical velocity $w = D\eta/Dt$, where $D/Dt = \partial/\partial t + U\partial/\partial x$ is the advective time derivative, and η is the vertical displacement. Since $\tilde{w}$ and $\tilde{\eta}$ are related by $\tilde{w} = -\iota\hat{\omega}\tilde{\eta}$, all of the solutions that we have derived for $\tilde{\eta}$ need only to be multiplied by $-\iota\tilde{\omega}$ to obtain the solution $\tilde{w}$. An inverse Fourier transform of $\tilde{w}$ gives the spatial solution w.

For the Fourier-ray model, the solution is computed by a discrete Fourier-series approximation to the inverse Fourier transform, for a spatial grid of 512 points in both x and y. (The vertical cross sections in Fig. 2 were computed at a 1-km vertical grid spacing.)

For the numerical model, there are 256 grid points in each horizontal direction, and 32 grid points in the vertical direction, with a grid spacing of 1 km in all directions. There are absorbing sponges near the top and lateral boundaries of the numerical model. The sponge near the top boundary is based on a Rayleigh friction, with the form $R_v q'$ in the governing equations. Here q' is a perturbation quantity (velocity or potential tem-
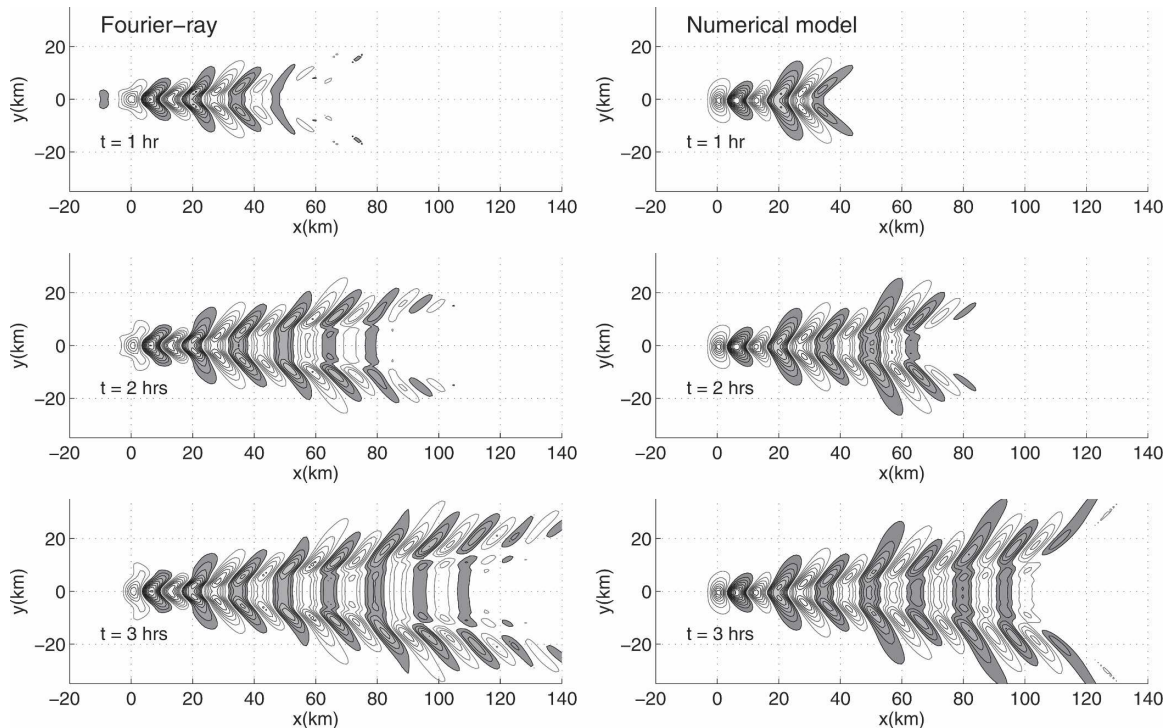
FIG. 1. Comparison of (left) the Fourier-ray solution and (right) the numerical model solution for the vertical velocity w in the WSK model, after 1, 2, and 3 h. The solutions are plotted at $z = 2.5$ km. Shaded contours are positive, the zero contour is omitted, and the contour interval is 0.025 m s^{-1}.

perature), and the damping coefficient R_v increases linearly with z in the top quarter of the model domain to a peak value of 0.004 s^{-1}. The sponge near the lateral boundaries has the form $R_h \nabla^2 q'$, where R_h increases linearly across the final 10 horizontal grid points, to a peak value of 4500 m^2 s^{-1}.

Figure 1 shows a comparison of (left panels) the Fourier-ray solution and (right panels) the numerical model solution for the vertical velocity w at $z = 2.5$ km and at times $t = 1$, 2, and 3 h. The range of values is about -0.21 to 0.25 for the numerical model, and about -0.19 to 0.23 for the Fourier-ray method. These ranges are established by $t = 1$ h. The numerical model gives peak values that are a few percent higher than those of the Fourier-ray method, even though the Fourier-ray method is inviscid and the numerical model has some numerical dissipation (though no explicit dissipation outside the sponge regions). We are not sure why this is the case, but we did check to see whether evanescent modes (with $\hat{\omega} > N$ at the ground) could account for the difference in peak values. We calculated the uniform solution for evanescent modes in the steady-state limit, but their magnitude was insignificant except at closer distances to the mountain. The results plotted here exclude these evanescent modes.

The *steady-state* Fourier-ray solution corresponding

to Fig. 1 here was given in Fig. 6 of Broutman et al. (2003). The steady-state solution has an amplitude range for w of -0.18 to 0.21, which is slightly smaller than the range predicted here by the transient Fourier-ray solution. This difference is a result of the damping used in the steady-state solution to remove the resonant singularity for the trapped waves.

Figure 1 also shows good agreement of the predictions for the horizontal extent of the wave field. For example, at $t = 2$ h, the mountain waves in both the Fourier-ray solution and the numerical solution extend about four wavelengths downwind of the mountain before starting to decay rapidly with distance, beyond about $x = 60$ km. Near this leading edge of the wave field, the initial rays make the dominant contribution to the solution, and the Fourier-ray method is likely to be inaccurate. This is due to our simple procedure for giving the initial rays the full wave amplitude of the steady-state solution, and also to our use of the rounding in (29).

At $t = 1$ h, the Fourier-ray method predicts anomalous wave amplitudes in the region upwind of the mountain ($x < 0$), where there is an extra leading crest (shaded contour) that does not occur in the numerical solution. The reason for this may be that during these early stages of the wave field development, a larger
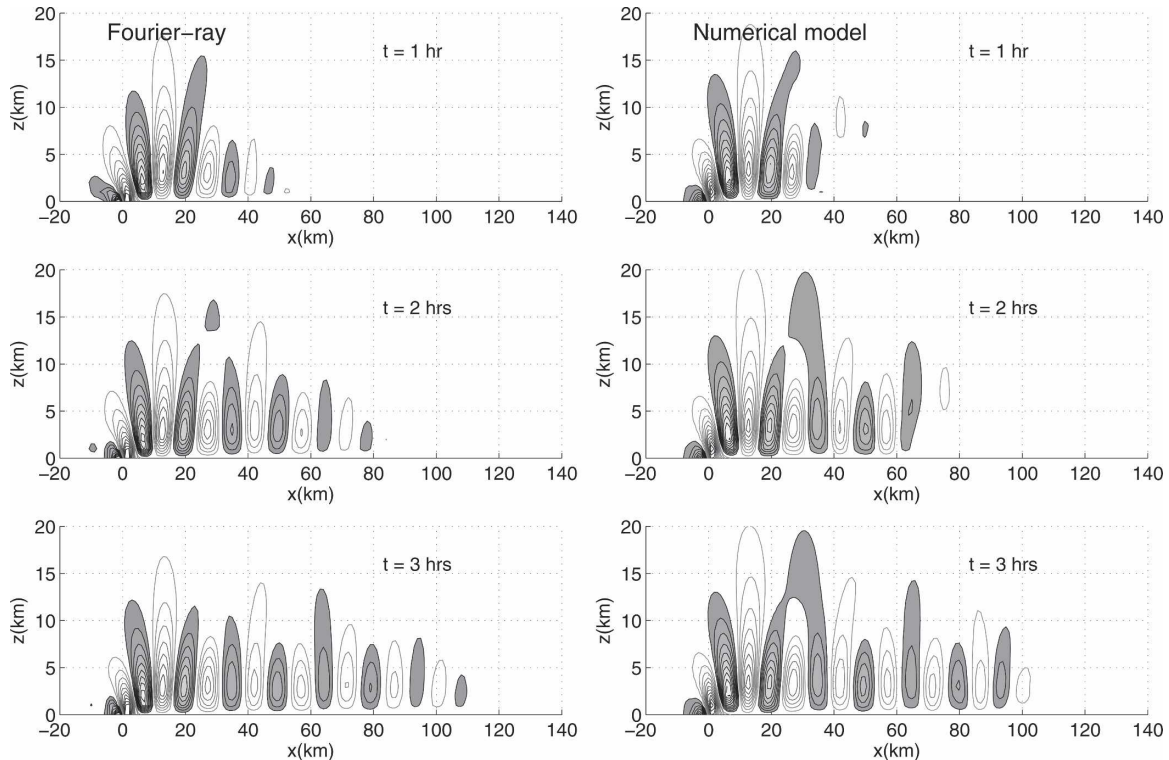
Fig. 2. Same as in Fig. 1, but for the vertical cross section at $y = 0$.

fraction of the rays have just been switched on to full steady-state amplitude in the ray tracing, which would cause some "ringing" in the spatial solution near the edges of the wave field. As time increases, more rays are correctly represented by the steady-state amplitudes, and the anamolous upwind crest disappears, as the plots indicate.

Figure 2 shows the same solutions as in Fig. 1, but in vertical cross section at $y = 0$. Again there is good agreement between the Fourier-ray solution and the numerical model solution.

4. Summary

We used ray tracing in a Fourier-transform domain to calculate the wave amplitudes and wave phase, and to estimate wave propagation times in order to account for wave transience. These ray solutions were then Fourier synthesized to compute the spatial solution. We considered an initial value problem in which the flow is started abruptly from rest, and the initial rays (and all subsequent rays) are assigned the full wave amplitude of the longtime steady-state solution. This gave good agreement with the predictions of a nonlinear mesoscale model in an example taken from WSK. A case with realisitic topography, winds and stratification is

considered by Eckermann et al. (2006), who provide comparisons of the transient Fourier-ray method with numerical simulations and satellite observations.

REFERENCES

Broad, A., 1999: Do orographic gravity waves break in flows with uniform wind direction turning with height? *Quart. J. Roy. Meteor. Soc.,* **125,** 1695–1714.

Broutman, D., and J. W. Rottman, 2004: A simplified Fourier method for computing the internal wavefield generated by an oscillating source in a horizontally moving, depth-dependent background. *Phys. Fluids,* **16,** 3682–3689.

——, ——, and ——, 2002: Maslov's method for stationary hydrostatic mountain waves. *Quart. J. Roy. Meteor. Soc.,* **128,** 1159–1172.

——, ——, and S. D. Eckermann, 2003: A simplified Fourier method for nonhydrostatic mountain waves. *J. Atmos. Sci.,* **60,** 2686–2696.

Brown, M. G., 2000: The Maslov integral representation of slowly

varying dispersive wavetrains in inhomogeneous moving media. *Wave Motion,* **32,** 247–266.

Eckermann, S. D., D. Broutman, J. Ma, and J. Lindeman, 2006: Fourier-ray modeling of short wavelength trapped lee waves observed in infrared satellite imagery near Jan Mayen. *Mon. Wea. Rev.,* **134,** 2830–2848.

Gjevik, B., and T. Marthinsen, 1978: Three-dimensional lee-wave pattern. *Quart. J. Roy. Meteor. Soc.,* **104,** 947–957.

Hines, C. O., 1988: On ray paths in mountain waves. *J. Atmos. Sci.,* **45,** 323–326.

Kravtsov, Y. A., and Y. Orlov, 1999: *Caustics, Catastrophes, and Wave Fields.* Springer, 216 pp.

Lighthill, M. J., 1978: *Waves in Fluids.* Cambridge University Press, 504 pp.

Lipps, F., and R. Hemler, 1982: A scale analysis of deep moist convection and some related numerical calculations. *J. Atmos. Sci.,* **39,** 2192–2210.

Lott, F., and H. Teitelbaum, 1993: Linear unsteady mountain waves. *Tellus,* **45A,** 201–220.

Maslov, V. P., and M. E. Fedoriuk, 1981: *Semi-Classical Approximation in Quantum Mechanics.* D. Reidel, 301 pp.

Shutts, G. J., 1998: Stationary gravity-wave structure in flows with directional wind shear. *Quart. J. Roy. Meteor. Soc.,* **124,** 1421–1442.

Smith, R. B., S. Skubis, J. D. Doyle, A. S. Broad, C. Kiemle, and H. Volkert, 2002: Mountain waves over Mont Blanc: Influence of a stagnant boundary layer. *J. Atmos. Sci.,* **59,** 2073–2092.

——, Q. Jiang, and J. D. Doyle, 2006: A theory of gravity wave absorption by a boundary layer. *J. Atmos. Sci.,* **63,** 774–781.

Wurtele, M. G., R. D. Sharman, and T. L. Keller, 1987: Analysis and simulations of a troposphere–stratosphere gravity wave model. Part I. *J. Atmos. Sci.,* **44,** 3269–3281.